Continuous Chirality Analysis of Model Stone−Wales Rearrangements in Fullerenes

Y. Pinto,[†,‡] P. W. Fowler,*[,§,||] D. Mitchell,[§] and D. Avnir*[,†,⊥]

Institute of Chemistry and Lise Meitner Minerva Center for Computational Quantum Chemistry, The Hebrew University of Jerusalem, Jerusalem 91904, Israel, and Department of Chemistry, University of Exeter, Exeter EX4 4QD, U.K.

Received: March 18, 1998

The Stone−Wales rearrangement is analyzed using a newly developed continuous chirality measure. In enantiomerization reactions of chiral fullerenes we find an approximately linear correlation between π-energy and the chirality content of the molecule. These correlations show that the sensitivity to chirality change increases for larger fullerenes. We show its predictive properties and provide an explanation for it on the basis of another observation; namely, that the chirality value decreases monotonically with fullerene size. Comparison of the enantiomerization to other isomerizations of fullerenes is made.

1. Introduction

We analyze in this report energy/chirality correlations along the Stone−Wales (SW)[1] rearrangement routes of fullerenes. As a possible route for interconversion of fullerene isomers, the SW (pyracylene) rearrangement (Figure 1) has attracted much attention from experimentalists and theorists.[2−11] Although it has a high activation energy, as is to be expected of a Woodward−Hoffmann thermally forbidden process,[4,9,11] its ability to move pentagonal rings on the surface of the fullerene may furnish the annealing step required in both pentagon-road[12] and fullerene-road[13,14] models of C_{60} formation and may account for the fact that the experimental product for higher fullerenes contains few isomers, and these generally the most stable of their class. SW maps displaying the interconnections allowed under this mechanism have been derived for many fullerenes, and all possible interconversions by this route for general fullerenes C_{20}−C_{50} and isolated-pentagon fullerenes C_{60}−C_{100} are listed in ref 7. An energetic dimension has been added to the maps for C_{40}, C_{60}, and C_{84}, concentrating on well depths rather than barrier heights.[15] Energetic analysis of the pathway with identification of the energy, symmetry, and structure of the transition state has been carried out for specific cases[4,9,11] and used to suggest a modification of its geometric details, although no topologically distinct variant with a lower activation energy has yet been proposed. Catalysis by temporary incorporation of other atoms has been suggested.[16]

We report here the utilization of a continuous symmetry measure (CSM)[17−20] as a reaction coordinate, allowing one to correlate the changes in the quantitative degree of chirality of a set of fullerenes with their π-energy throughout SW automerizations, enantiomerizations, and isomerizations. The present paper takes the study of the symmetry aspects of the SW rearrangement a step further, applying this newly developed conceptual and mathematical tool to model the reaction pathway based on Hückel theory. It will be seen that even this drastically simplified model can afford novel insight into general features of fullerene-to-fullerene isomerization when correlated to the degree of chirality. In particular we find linear correlations between chirality and π-energy in enantiomerization reactions

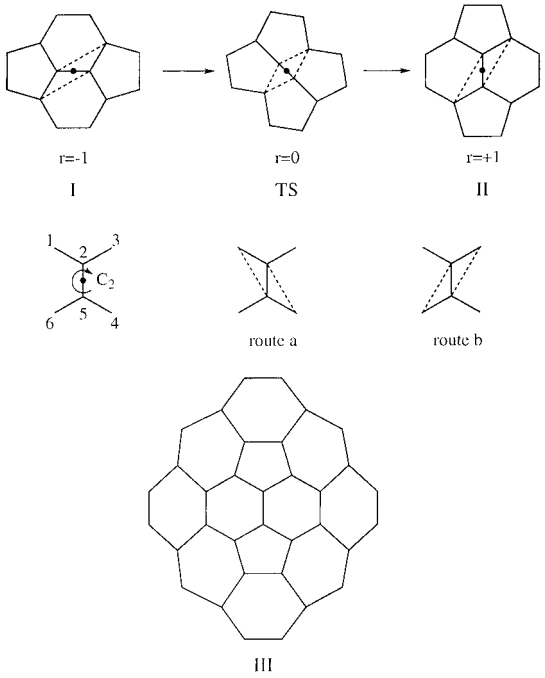

Figure 1. Stone−Wales transformation requires the presence of a four-ring motif on the surface of the reactant fullerene. This patch consists of two hexagons and two pentagons arranged as in **I**. Notional rotation of the central ("Stone−Wales" or "SW") 2−5 bond through $\pi/2$ rad along with the breaking of its 2−3 and 5−6 bonds and the forming of the 3−5 and 2−6 connections exchanges the pentagons and hexagons, producing a "rotated" patch within the same perimeter of 12 atoms and 12 bonds (structure **II**). Within the Hückel model, the bond parameters are $\beta_{23} = \beta_{56} = {}^1/_2\,(1 - r)\beta$ and $\beta_{35} = \beta_{26} = {}^1/_2\,(1 + r)\beta$ where r runs from -1 to $+1$. The product frame is also a fullerene, though not necessarily distinct from the reactant, and the outcome of the transformation is independent of the sense of rotation of the SW bond. Within the Hückel approximation, the transition state (TS) is highly symmetric. An isolated pentagon fullerene may isomerize in an SW reaction if it has the Stone−Wales patch embedded in it (structure **III**).

† The Hebrew University of Jerusalem.
‡ E-mail: yariv@chem.ch.huji.ac.il.
§ University of exeter.
|| E-mail: P.W.Fowler@exeter.ac.uk.
⊥ E-mail: david@chem.ch.huji.ac.il.

S1089-5647(98)01546-6 CCC: $15.00
Published on Web 07/07/1998

of chiral fullerenes. We also find that the chirality content of fullerenes decreases exponentially with their size.

2. Stone−Wales Rearrangement of Fullerenes

The transformation requires a four-ring motif on the surface of the reactant fullerene that consists of two hexagons and two pentagons arranged as in **I** (Figure 1). Notional rotation of the central bond (SW bond) together with its connections through $\pi/2$ rad exchanges the pentagons and hexagons, producing a "rotated" patch, **II**, within the same perimeter of 12 atoms and 12 bonds. The product cage is also a fullerene, though not necessarily distinct from the reactant, and the outcome of the transformation is independent of the sense of the rotation of the SW bond. A given fullerene cage may support up to 30 different, though not necessarily symmetry-distinct, SW transformations. A restricted version of the transformation based on a larger patch (Figure 1, **III**) consisting of **I** embedded in a circuit of eight hexagons can be used to connect isolated-pentagon fullerenes with one another without passing through adjacent-pentagon intermediates.

Any particular SW transformation can be discussed in terms of the site symmetry of the patch and its active central bond. (The symmetry is understood here to be the maximal point group compatible with the molecular graph.)[21] As an edge of a polyhedral cage, the SW bond in the unperturbed patch has one of the four-site symmetries: C_{2v}, C_2, C_s, or C_1. Since this symmetry is unaffected by a full 90° rotation of the central bond, the patch site group is common to both endpoints of the reaction path, though not in general to the points between.

If the transformation is a simple rotation of the central bond about an axis passing perpendicularly through the patch, the rotational axis (C_2 or C_1) of the site group is preserved at all points along the reaction path. Any mirror symmetries of the site group are lost as soon as the SW bond starts to rotate, though, as we shall see, a new mirror plane or planes may appear in the transition state.

Although the product of a SW transformation is independent of the *sense* of the rotation, the energy profile of the pathway is not. In particular, the Hückel model we use here (see below) with clockwise and counterclockwise rotation of the SW bond will give distinct routes passing through two distinct transition states whenever the site group of the original patch lacks a mirror plane, i.e., when the site has the chiral C_2 or C_1 symmetry. The two transition states, though differing in energy, will share a common point group (which in each case will be the site group of the SW bond in the transition state and must therefore be C_{2v} or a subgroup).

So far, the discussion has concentrated on the site symmetry of the active SW patch. A number of patches on the fullerene surface may be equivalent: the size of such a set (or *orbit*) is the quotient (order of molecular point group)/(order of site group). Trivially, two fullerenes linked by the transformation must belong to point groups that have the site group of the active patch as a common subgroup.

Rotation of one of a set of symmetry-equivalent SW bonds may lead to (i) a distinct structural isomer (isomerization), (ii) a distinct enantiomer of the starting fullerene (enantiomerization), or (iii) a copy of the starting isomer (automerization). Isomerization is possible for all patch symmetries, but enantiomerization requires a chiral patch in a (chiral) fullerene and so is only possible for site symmetries C_2 and C_1. Cases of automerization identified so far for fullerenes involve inversion of configuration at a chiral patch in an achiral cage (e.g., C_1 in C_s) to produce the superimposable mirror image of the starting structure. Both automerization and enantiomerization are "spectrally neutral" in that they do not affect the eigenvalues of the adjacency matrix. No cases of cospectral but nonisomorphic fullerenes are known, and therefore all spectrally neutral transformations of achiral fullerenes are presumed to be automerizations.

A special feature of enantiomerizations within the present model should be pointed out. An enantiomerization could in principle proceed via an achiral or a chiral transition state. In the topological model, the transition state for an enantiomerization is located at the exact midpoint of the path and at this point the molecular graph has four half-bonds in the SW patch and a maximal point group that includes mirror symmetry. Within the model, therefore, the transition state is achiral. This limitation is not shared by more sophisticated models[9] and is not necessarily a feature of the real system.

Within the class of isomerizations, a SW transformation may relate two achiral fullerenes, two chiral or one chiral, and one achiral. Two mirror-image versions of each chiral-to-chiral connection on the SW map will exist; i.e., if A goes to B, then its enantiomer $\bar{A}$ will go to $\bar{B}$. Perhaps more interesting are the achiral-to-chiral connections. As discussed in ref 5, symmetry dictates that if a given achiral fullerene A has *n* patches leading to the chiral B, then it must have *n* leading to the enantiomer $\bar{B}$. Within each orbit any two patches that are exchanged by a proper rotation lead to the same enantiomer and any two exchanged by an improper operation to opposite enantiomers B and $\bar{B}$.

3. Computational Tools and Details

Hückel Model. A simple "topological" concerted model of the transformation can be constructed by representing the Hückel resonance integrals of the four breaking and forming bonds as linear functions of a reaction coordinate *r*, which runs from reactant at $r = -1$ to product at $r = +1$ (Figure 1). The π-energy (found by diagonalization of the weighted adjacency matrix) is then a function of *r*, giving a model of the barrier to the transformation.[3] However, as changes in the SW bond itself and the distortion of the σ framework are neglected, the energy profile is necessarily crude. This Hückel calculation also provides a model for the geometry and symmetry changes along the pathway, since topological coordinates may be calculated from the eigenvectors of the weighted adjacency matrix at each value of *r*.[21]

Detailed calculations of the motion of atoms during the rearrangement using more sophisticated all-electron methods show that the in-plane rotation implied by the Hückel calculation is oversimplified and gives rise to too high a symmetry in the transition state.[4,9] Nevertheless, the qualitative height and position of the barrier are not grossly altered by the assumption of high symmetry.[4]

In the current paper we explore the Hückel model energetics of the distinct pathways in some typical cases and display the correlations between changes in energy and symmetry along the paths. The mathematical tool that we use to keep track of the appearance and disappearance of symmetry elements is the continuous symmetry measure (CSM), described next.

Continuous Symmetry Measure. The need for symmetry and chirality metrics has been addressed by a number of research groups,[22−33] including our own.[17−20] Aiming at versatility, convenience, and conformance with chemical and physical intuition, we have developed the continuous symmetry measure (CSM)[17−19] and the related continuous chirality measure (CCM)[20] methodologies, which carry the following messages.

First, the structural chemistry is too rich to be described with the coarse binary language of having or not having the property of being symmetric or achiral. Second, it agrees with chemical, biochemical, and physical intuition to ask questions such as "Given a set of chiral molecules, by how much do they differ from each other in their achirality content?" And third, the problem of how to quantify these structural properties is solvable; a concept of what is exactly to be measured was provided and the practice of carrying it out was detailed and demonstrated. This approach already proved to be useful in a number of symmetry/chirality related issues, including the application of the symmetry measure as an order parameter in small clusters,[34] a quantitative investigation of the chirality properties of the cyclic trimer of water and of its enantiomerization pathways,[35] an analysis of the correlation between the degree of centrosymmetricity and hyperpolarizability,[36] a quantitative analysis of the chirality of large random objects,[37] and an analysis of the macroscopic chirality of Pasteur's tartrate crystals.[38]

Our solution for quantifying symmetry in general, and chirality as a special case of asymmetry, has been described in detail elsewhere.[39,40] Its main features are outlined briefly here. In essence, CSM is a distance measure that quantifies the minimal translation that each vertex of a structure has to undergo in order to attain a desired symmetry. It is a special distance function in that there is no ideal reference structure a priori, but the nearest structure with the desired symmetry is calculated (according to special algorithms). In a formal way, given n vertexes of the original configuration located at P_i and given a symmetry point group G, the amount $S'(G)$ of this symmetry in this configuration is

$$S'(G) = \frac{1}{nD^2}\sum_{i=1}^{n}||P_i - \hat{P}_i|| \tag{1}$$

where $\hat{P}_i$ are the corresponding points in the nearest G-symmetric configuration. To avoid size effects, the original structure is normalized to the distance from the center of mass of the structure to the farthest vertex D, i.e., it is accomplished by division of all vertex distances of the object by the farthest distance from the center of mass (i.e., that distance becomes 1; other normalizations, such as rms, are possible). Thus, in the center-of-mass coordinates, the normalization factor takes the form

$$D = ||P^{\text{farthest}}|| \tag{2}$$

If a shape has the desired symmetry, $S(G) = 0$, and $S(G)$ increases as the shape departs from G symmetry up to a maximal value smaller or equal to 1. Equation 1 is general and allows one to evaluate the symmetry measure of any shape relative to any symmetry group or element. The main theoretical and computational task in applying eq 1 has been to find the set of $\hat{P}_i$, the solution to which is described in ref 18. It is based on folding the original vertices, $\{P_i\}$, averaging the folded cluster, and unfolding into the symmetric shape, $\{\hat{P}_i\}$.

A particular family of symmetry point groups of relevance to this report are the achiral ones; namely, all groups that contain improper elements G_{improper}, such as reflection, inversion, and even-numbered improper rotations. In these cases $S(G)$ is a measure of chirality, (the continuous chirality measure—CCM[20]). In its simplest form, the measure of chirality is the minimal distance of the object from having a symmetry mirror plane. The CCM is defined as

$$S'(\text{chirality}) = \min[S'(G_{\text{improper}})] \tag{3}$$

Note that the maximal value of S in eq 3 never reaches 1 because the distance to a plane is always smaller than the distance to a center point. Finally, since in most practical questions encountered and analyzed the structures in question are not very far from the relevant symmetry, we found it convenient to expand the scale by a factor of 100:

$$S(\text{G}) = 100S'(G) \tag{4}$$

The CSM value depends on the structure and topology (connectivity) of the object. Thus, equivalent structures having different topologies may possess different chirality values.

Selection and Representation of the SW Isomerizations. With the preliminaries of method and general symmetry considerations over, we now turn to a series of examples of hypothetical SW rearrangements in particular fullerenes. All mathematically possible SW transformations for the general fullerenes C_n in the range $20 \le n \le 50$ have been tabulated, as have all those in which both reactant and product are isolated-pentagon fullerenes in the range $60 \le n \le 100$. Many SW links exist among the fullerene molecular graphs in these ranges, and lists of the separate families of interconverting isomers and maps of the connections within them are also given in ref 7.

If an eigenvalue criterion is used for classification and all transformations A → B or $\bar{\text{B}}$ are lumped together regardless of symmetry equivalence or otherwise, there are 1695 distinct SW isomerizations of fullerenes in the range $20 \le n \le 50$ and 85 distinct spectrally neutral transformations A → A or $\bar{\text{A}}$. Of the latter, only two can be immediately identified as automerizations by virtue of the achirality of A; these are transformations of 34:2 (see Figure 11) and 46:2 (the first number denotes the number of carbons and the number after the colon is the serial notation in the spirally ordered Atlas of Fullerenes[7]), which are both fullerenes of C_s symmetry.

In the examples to be discussed, an exactly similar procedure was followed in every case. Each distinct reaction pathway was represented by a discrete grid of the parameter r with spacing 0.1. At each point the cage geometry was calculated as a set of topological coordinates. These are Cartesian coordinates derived from the eigenvectors of the weighted adjacency matrix according to the recipe

$$x_s = c_s^{(2)}/\sqrt{\epsilon_1 - \epsilon_2} \tag{5}$$

$$y_s = c_s^{(3)}/\sqrt{\epsilon_1 - \epsilon_3} \tag{6}$$

$$z_s = c_s^{(4)}/\sqrt{\epsilon_1 - \epsilon_4} \tag{7}$$

where $c_s^{(i)}$ is the coefficient of vector i on atom s and ϵ_i is its eigenvalue. The vectors are ordered by eigenvalue so that ϵ_1 belongs to the nodeless "S" and ϵ_2, ϵ_3, ϵ_4 (usually) to the singly noded "P" combinations. An overall scaling factor can be applied to give a particular desired average bond length, but the properties calculated here are independent of the distance scale. (For especially anisotropic fullerene isomers, it may be necessary to search beyond the third and fourth vectors to find all three singly noded "*P*"-like combinations.)

4. Results

I. Enantiomerization of Chiral Fullerenes C_{28} and C_{32}. The smallest fullerene isomer to support a SW rearrangement is 28:1 which belongs to the D_2 point group and is converted

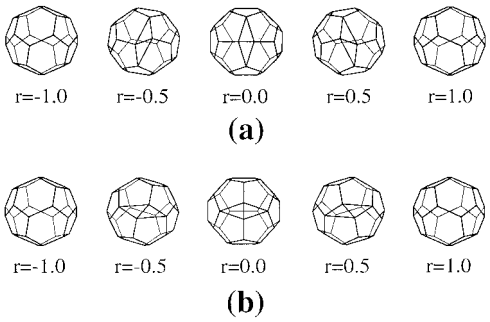

Figure 2. Sequence of polyhedra predicted by the Hückel model of the Stone−Wales transformation for the enantiomerization of D_2 C_{28}. Snapshots are shown for the range $r = -1$ to $r = +1$ in steps of 0.5. The transition state represented by $r = 0$ eclipses the two SW bonds in route a (a) and staggers them in route b (b).

to its enantiomer by rotation of either one of the two equivalent SW bonds, each of which has C_2 site symmetry. In agreement with the general points made above about symmetry and the topological model, the C_2 axis is preserved during the SW rotation. Note that clockwise and counterclockwise rotations lead to different transition states that must share, however, the same achiral point group; since the mirror planes that develop while approaching the transition states contain the C_2 axis, both states must have C_{2v} symmetry (Figure 2). They can be distinguished in this case by the spatial relationship between the active and inactive SW bonds at the transition point: route a leads to eclipsing of these bonds, route b to staggering. Figure 2 shows the sequence of polyhedra along each route as obtained from the eigenvectors of the weighted adjacency matrix and illustrates the topological difference between the two transition states. In the topological model, the π-energy profiles $E_\pi(r)$ are similar for both routes, with barrier heights of $0.44|\beta|$ for route a and $0.31|\beta|$ for route b (see Figure 3a). The energy profiles are replotted in Figure 3b against the symmetry measure $S(C_s)$ that tracks the development of a vertical mirror plane, with a remarkable result: a nearly linear correlation between energy and symmetry is obtained. We refer to this result in the discussion.

Both planes of the appropriate C_{2v} group develop at the same rate so that similar curves would be found for a full C_{2v} measure, $S(C_{2v})$. However, since the two routes have different topologies (connectivities), the planes being tracked by $S(C_s)$ are different in each case (Figure 2 at $r = 0.0$). At each point on either route the nearest symmetric polyhedron has full C_{2v} symmetry.

The argument that accounts for the ordering of the curves $E_\pi(r)$ for the two routes is that the initial slopes for the patch of C_2 symmetry in Figure 2a are

$$(\mathrm{d}E_\pi/\mathrm{d}r)_\mathrm{a} = 2(P_{1,5} - P_{1,2})\beta \tag{8}$$

$$(\mathrm{d}E_\pi/\mathrm{d}r)_\mathrm{b} = 2(P_{3,5} - P_{3,2})\beta \tag{9}$$

where $P_{s,t}$ is the π bond order between atoms s and t in the unperturbed molecule. In D_2 C_{28}, $P_{1,2} = 0.4492$, $P_{1,5} = 0.0152$, $P_{3,2} = 0.3945$, $P_{3,5} = 0.0700$ so that the energy is initially rising 1.34 times faster for route b.

One qualitative difference between routes a and b is the behavior of the HOMO−LUMO gap Δ as a function of r. As Figure 3c shows, the gap changes hardly at all along route a but widens by 273% between the initial cage and the transition state along b, owing to the sensitivity of the LUMO energy to motion along this route. The difference in behavior can be rationalized by a perturbation argument. In first order, the change in a fullerene orbital energy ϵ with rotation of the central bond of the SW patch depends on the coefficients of the unperturbed orbital on the four atoms defining the rhombus of breaking and forming bonds (i.e., {1, 2, 5, 4} in route a and {2, 3, 5, 6} in route b as shown in Figure 1). In the topological model the derivative $(\mathrm{d}\epsilon/\mathrm{d}r)$ is therefore $(c_4 - c_1)(c_2 - c_5)\beta$ for route a and $(c_6 - c_3)(c_2 - c_5)\beta$ for route b. Both expressions vanish for orbitals that are symmetric under C_2 rotation, as for example the HOMO of C_{28}, since for such orbitals $c_2 = c_5$. The LUMO of C_{28}, on the other hand, is antisymmetric under C_2 and has $c_1 = -c_4 = 0.0071$, $c_2 = -c_5 = 0.2359$, $c_3 = -c_6 = 0.3178$, $(\mathrm{d}\epsilon/\mathrm{d}r)_\mathrm{a} = 0.0068$, $(\mathrm{d}\epsilon/\mathrm{d}r)_\mathrm{b} = 0.3000$. Motion along route b is therefore expected to produce a large change in ϵ_{LUMO} and hence Δ. We redraw the HOMO and LUMO energies of both routes against the chirality value in Figure 3d.

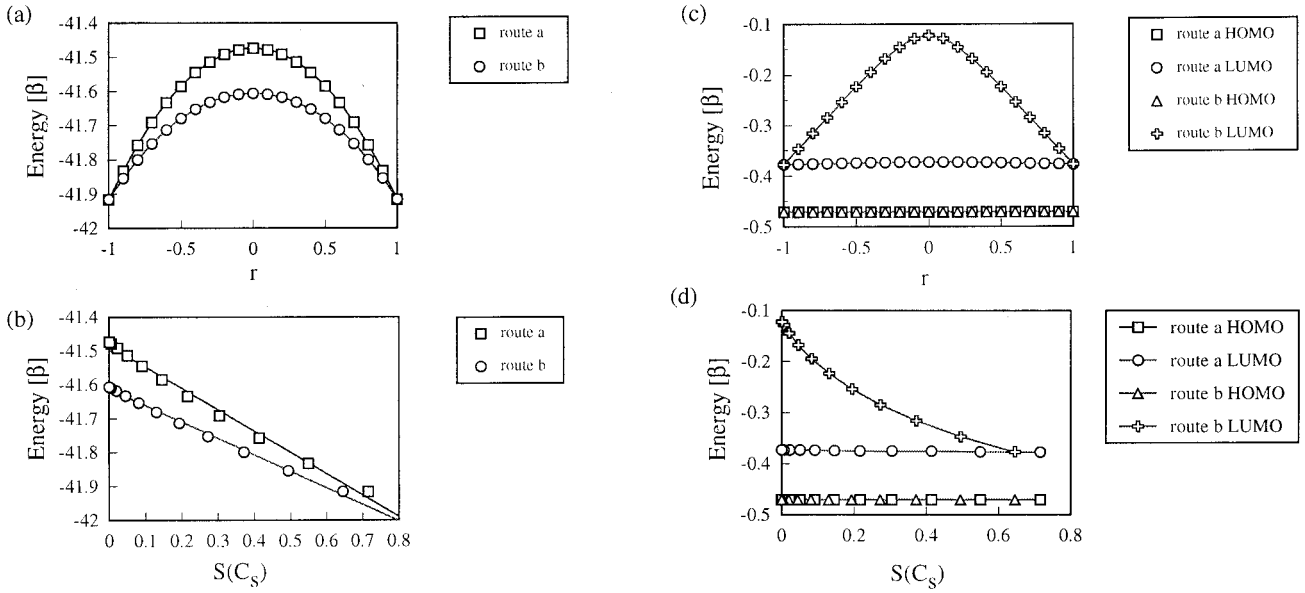

Figure 3. Hückel model of the Stone−Wales transformation of the D_2 isomer of C_{28}. Curves for routes a and b show total π-energy E_π ($|\beta|$) (a) as a function of r and (b) as a function of the measure $S(C_s)$, which indicates the distance from a configuration of mirror symmetry. The transition states have mirror symmetry indicated by $S(C_s) = 0$. (c) HOMO and LUMO energies ϵ ($|\beta|$) are shown as functions of the reaction coordinate r. The LUMO energy varies strongly for route b but hardly at all for route a, while variation of the HOMO energy is negligible for both routes. (d) HOMO and LUMO energies are replotted against $S(C_s)$.

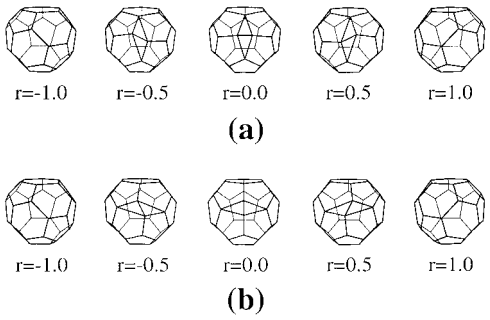

Figure 4. Sequence of polyhedra for the Hückel model of the enantiomerization of the C_{32} fullerene isomer 32:4. Route a (a) and route (b) are distinguished by the orientation of the SW bond relative to the pentagon across from it. Conventions are as in Figure 2.

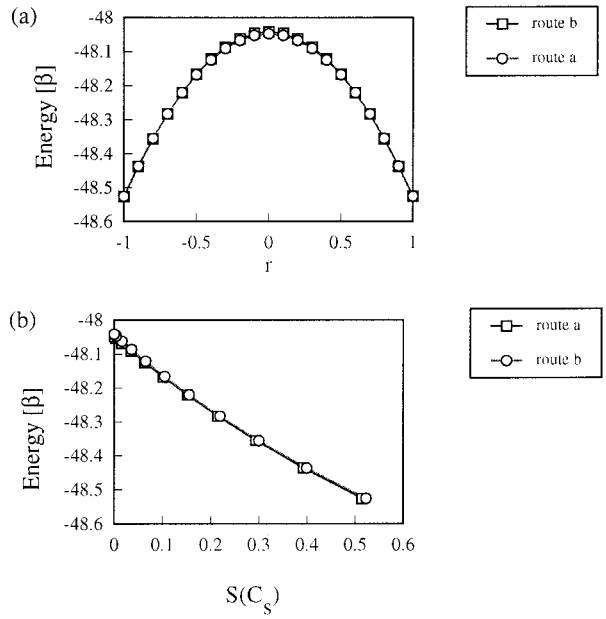

Figure 5. Enantiomerization of isomer 32:4 showing the variation of total π-energy E_π ($|\beta|$) with reaction coordinate (a) and mirror symmetry (b) for the route illustrated in Figure 4.

After C_{28} the next fullerene to support a SW enantiomerization is an isomer of C_{32}. The cage 32:4, which is of overall C_2 symmetry, has four SW bonds that fall into two sets of two, including one pair that leads to enantiomerization of the starting cage. Each member of this pair is of C_1 symmetry and by either clockwise or counterclockwise rotation the same product is obtained but via different C_s transition states that are distinguished by the relative orientation of the SW bond and the mirror plane (Figure 4). Both routes have very similar profiles $E_\pi(r)$ and $E_\pi(S)$ (Figure 5), and again, an approximate linear correlation between the Hückel π-energy and the chirality value exists.

II. Inequivalent Enantiomerizations in a Chiral C_{60} Fullerene. SW rotations of bonds that are related by a symmetry operation necessarily lead to either identical or mirror-image products. Occasionally, the rotations of inequivalent patches can also lead to the same product. Thus, 38:3 and 42:39 are of C_1 symmetry but both have two enantiomerization patches, 40:19 is of C_s symmetry but has three automerization patches, and further cases can be identified by the use of the transformation tables in ref 7.

Of these possibilities we selected to illustrate in Figure 6 the four possible routes for the enantiomerization of the C_1 isomer 60:1800. Figure 7 shows the energy and symmetry curves for all four. All transition states have, of course, C_s symmetry.

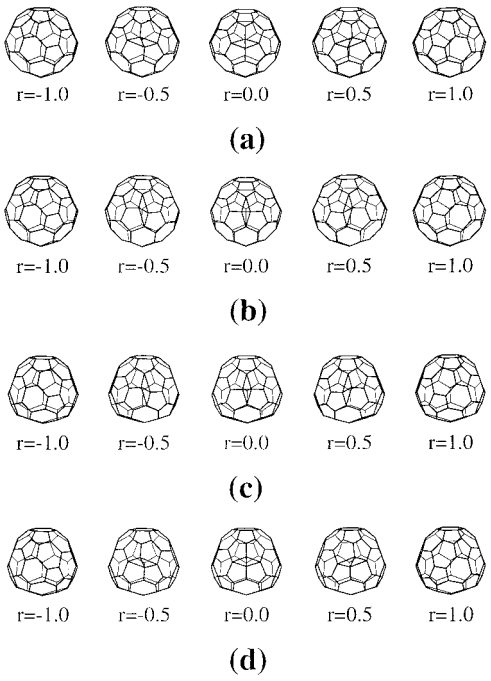

Figure 6. Sequence of polyhedra for the Hückel model of the enantiomerization via two patches of 60:1800 (by two distinct routes based on each patch). Conventions are as in Figure 2.

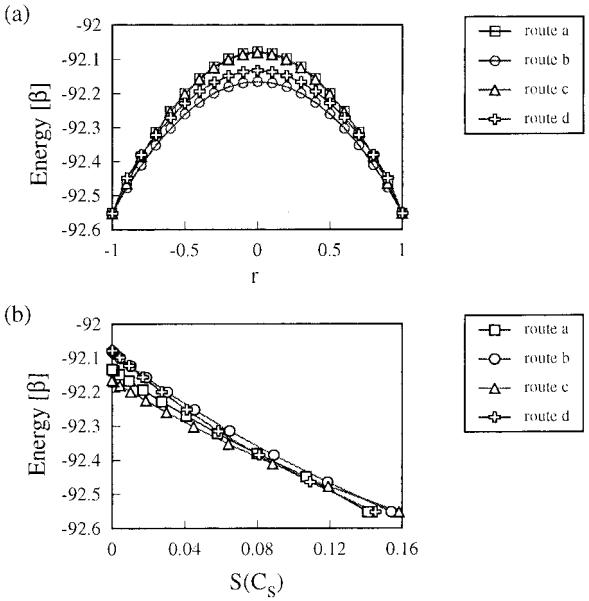

Figure 7. Energy profiles for the inequivalent enantiomerizations of 60:1800 illustrated in Figure 12. Conventions are as in Figure 3.

III. SW Transformations of C_{34} Fullerenes. Among the 13 transformations of the six distinct structural isomers of C_{34} fullerenes there are three that are spectrally neutral. Of these, two are enantiomerizations (of 34:4 and 34:5) and one, 34:2, is the smallest possible fullerene automerization.

The enantiomerizations of 34:4 and 34:5 (Figures 8 and 9, respectively) both proceed by rotation of a patch in a C_2 fullerene but are otherwise quite different. In the first, the clockwise and counterclockwise rotations of a C_1 patch give almost identical $E_\pi(r)$ profiles and intersecting symmetry curves $E_\pi(S)$ (Figure 10). In the second, the patch has C_2 symmetry, the $E_\pi(r)$ profiles are better separated, and the curves $E_\pi(s)$ are almost parallel. The symmetry of the transition states differs too: for 34:4 it is C_s and for 34:5 it is C_{2v}.

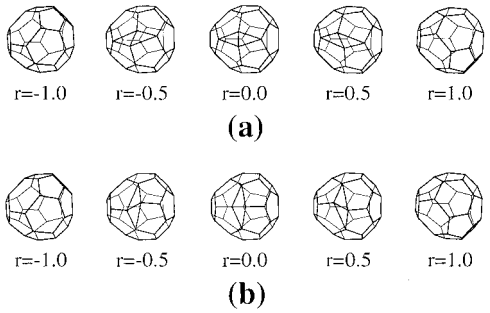

Figure 8. Sequence of polyhedra for the Hückel model of the enantiomerization of the C_{34} fullerene isomer 34:4 Conventions are as in Figure 2. The two distinct routes are shown.

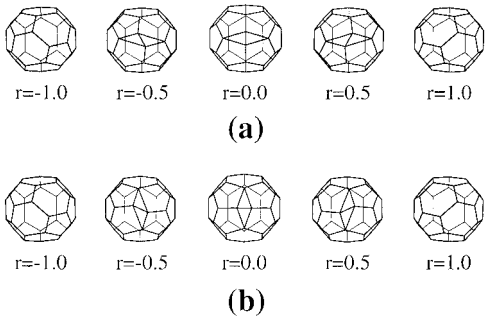

Figure 9. Sequence of polyhedra for the Hückel model of the enantiomerization of the C_{34} fullerene isomer 34:5. Conventions are as in Figure 2. The two distinct routes are shown.

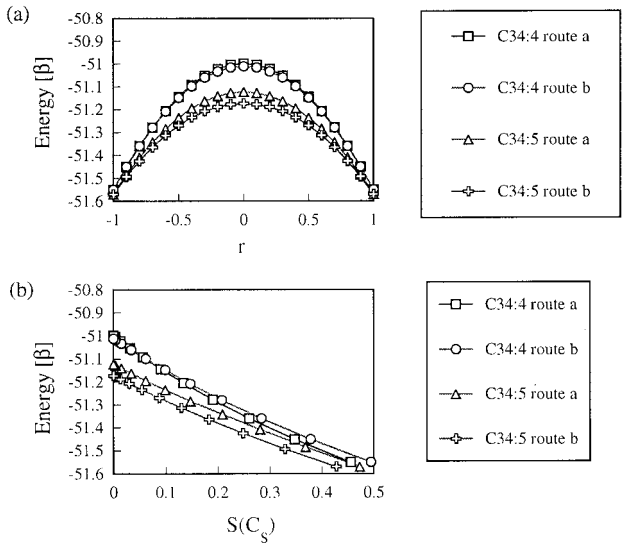

Figure 10. Energy profiles for the Stone−Wales enantiomerizations of the 34:4 and 34:5 isomers (illustrated in Figures 10 and 11, respectively). Conventions are as in Figure 3.

The 34:2 (the smallest fullerene automerization) has C_s symmetry and three pairs of SW bonds (all therefore of C_1 site symmetry) of which one pair leads back to the starting isomer. The clockwise and counterclockwise routes go over distinct C_s transition states that both give the (superimposable) mirror image of the starting cage (Figure 11) but are well separated in transition-state energy (Figure 12). We track both the σ-plane of the starting (and ending) cage and that of the transition state. The chirality value is the smaller of the two values ($S(C_s) = \min[S(C_s^{GS}), S(C_s^{TS})]$). Both routes have a point of maximum chirality (i.e., a point equidistant from both appearing and disappearing symmetry planes) that is neither reactant nor product.

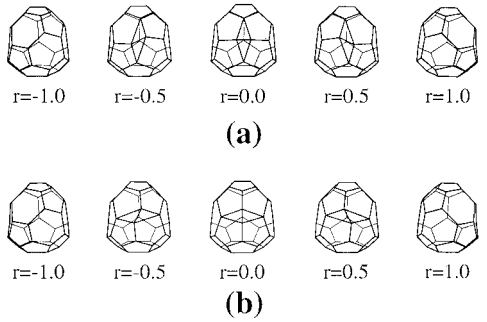

Figure 11. Sequence of polyhedra for the Hückel model of the automerization of the C_{34} fullerene isomer 34:2. Conventions are as in Figure 2. The two distinct routes are shown. Note that 34:2 has C_s symmetry and so does the transition state.

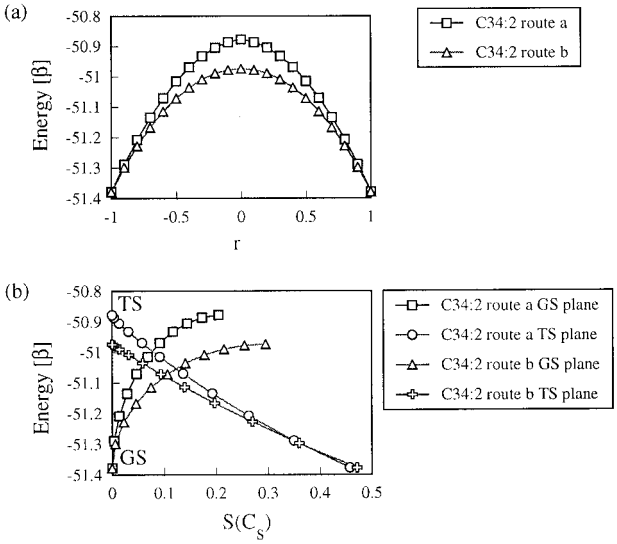

Figure 12. Energy profiles for the Stone−Wales automerization of the C_{34} fullerene isomer 34:2. The CCM is used to track the distance to both the symmetry planes of the starting cage (GS) and of the transition state. The chirality value is the smaller of the two.

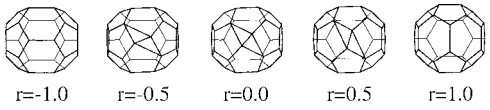

Figure 13. Sequence of polyhedra for the Hückel model of the isomerization 30:1 (D_{5h}) → 30:2 (C_{2v}). Conventions as Figure 2. Note that the transition state does not coincide with $r = 0$ (see Figure 7), and there is now only one distinct route because the site symmetry of the SW patch has a symmetry plane, making clockwise and counterclockwise rotations of the SW bond equivalent.

IV. Isomerization of Fullerenes C_{30}. In the canonically ordered spiral catalog,[7] the first possible SW transformation after the enantiomerization of 28:1 is between isomers 30:1 and 30:2. Isomer 30:1 is cylindrical, with two hemidodecahedral caps separated by a belt of five parallel hexagons in an arrangement of D_{5h} symmetry. Every hexagon−hexagon fusion is therefore a SW bond bisected by the equatorial σ_h plane. The site symmetry of each is C_{2v}, and rotation of any one leads to the same product, the C_{2v} fullerene 30:2.

Figure 13 shows the topological model of the pathway from 30:1 to 30:2. In keeping with the achirality of the starting site symmetry, clockwise and counterclockwise twists of the central SW bond lead to mirror-image pathways with identical energy profiles. Since reactant and product are distinct structural isomers, the transition state defined by the vanishing of the

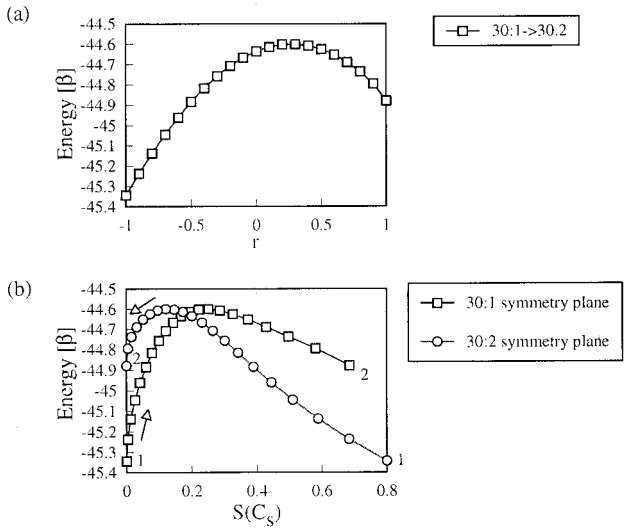

Figure 14. Hückel model of the Stone−Wales isomerization 30:1 → 30:2 illustrated in Figure 13. Here, as described in the text, the reaction route on the symmetry profile runs from the point labeled 1 on the vertical axis out to the intersection of the curve and back to the vertical axis at the point labeled 2. The two curves (b) follow the symmetry value of the two topologies of 30:1 and 30:2.

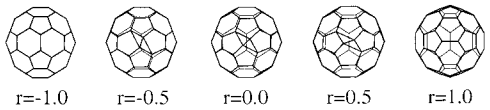

Figure 15. Sequence of polyhedra for the Hückel model of the Stone−Wales transformation of the icosahedral isomer of C_{60} (60:1812) to the C_{2v} isomer with two pentagon adjacencies (60:1809). Conventions are as in Figure 2. There is only one distinct route, and the point $r = 0$ is not the transition state in this transformation.

derivative (dE/dr) is not at $r = 0$; in the Hückel model it lies at $r \cong 0.3$, i.e., to the product side (Figure 14a).

We use the continuous symmetry measure $S(C_s)$ to track the synchronous disappearance of the two mirror planes of the reactant and the simultaneous synchronous appearance of the two of the product (Figure 14b). In this figure, the course of the reaction 30:1 → 30:2 follows the lower curve down from reactant ($E_\pi = -45.343\beta$, $S(C_s) = 0$) to the point of maximum chirality at the intersection of the curves, then follows the upper curve back to the product on the vertical axis ($E_\pi = -45.880\beta$; again $S(C_s) = 0$). A plot of the *chirality measure* $S(G_{\text{improper}})$ (the nearest G_{improper} is always C_s in the case of this kind of reaction in fullerenes, since the reaction patch is a unique feature on the cage; such a feature must include the improper symmetry element) against r would therefore have a discontinuity of slope at $r \cong 0.5$ where the instantaneous configuration is equidistant in symmetry from the C_{2v} groups of both product and reactant. At each point on the path, however, the nearest C_s symmetric object has full C_{2v} point-group symmetry, matching one of the two topologies. Away from the immediate neighborhood of the switch, the two separate arms of the energy−CSM correlation are once more roughly linear.

V. Isomerization of Icosahedral C_{60}. We conclude our case analyses with the celebrated C_{60} fullerene. The SW transformation was first proposed in the context of nonicosahedral isomers of C_{60}. However, if the starting cage is I_h C_{60} (60:1812) itself, there is only one possible product, a C_{2v} cage (60:1809) with two pentagon adjacencies, which can be reached by rotation of any one of 30 equivalent SW bonds. The site symmetry in this case is C_{2v}, and the unique transition state is therefore of C_2 symmetry (Figure 15). Since the transformation connects

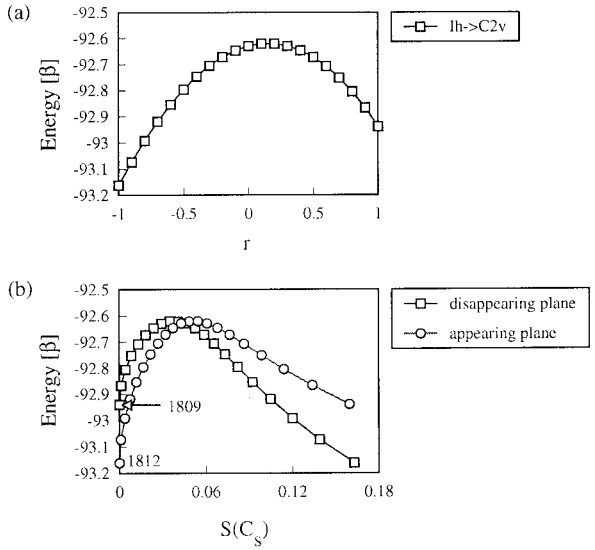

Figure 16. Energy profiles for the Stone−Wales isomerization of I_h C_{60}. Conventions are as in Figure 3. The reaction route on the symmetry profile runs from the point labeled 1812 on the vertical axis, out to the intersection of the curves, and back to the vertical axis at the point labeled 1809. 60:1812 is the icosahedral, isolated-pentagon isomer of C_{60}, 60:1809 the C_{2v} isomer with two pentagon fusions.

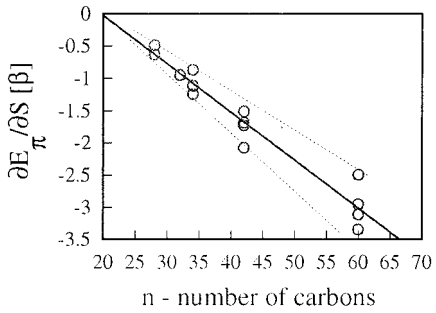

Figure 17. Plot of the π-energy-mirror symmetry slopes against the number of carbons in Stone−Wales enantiomerizations of fullerenes. An increase in the absolute value of the energy-symmetry slope for larger fullerenes is evident. The slopes were calculated for each enantiomerization path separately. The correlation between the average slope (for each size of fullerene) and the number of carbon atoms is linear with $dE_\pi/dS = -0.075n + 1.5$. By extrapolation we find that $dE\pi/dS$ becomes zero at C_{20}—the smallest possible fullerene (which is an achiral dodecahedron).

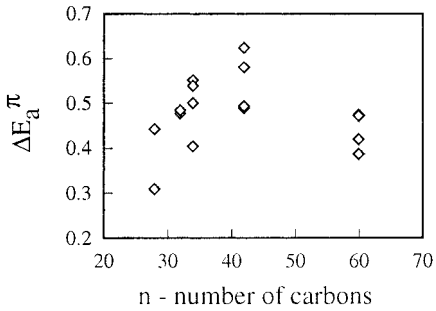

Figure 18. Plot of the energy barrier of the various enantiomerization paths against the number of carbons. In contrast to the data in Figure 16, no predictive pattern is revealed.

distinct structural isomers, the energy profile is not symmetrical about $r = 0$, and in this case the transition state is slightly closer to the I_h reactant. The most chiral point on the pathway is close to the transition state but on the product side (Figure 16).

In the simple topological model the barrier height is $0.541|\beta|$ from the I_h side. More sophisticated calculations give an explicit

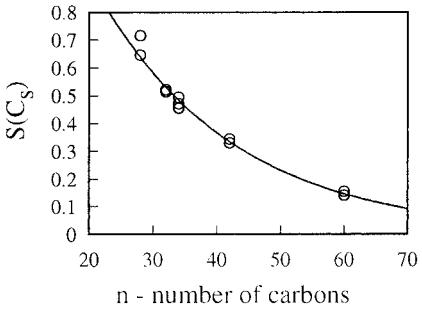

Figure 19. Chirality value of the reactant fullerene in enantiomerization reactions plotted vs the number of carbons. The fit found is exponential with $S(C_s) = 2.3e^{-0.046n}$. The chirality per carbon decreases slowly as the fullerene grows larger.

barrier of 6.2 eV but retain the C_2 symmetry of the topological transition state.

5. Discussion: Enantiomerization π-Energy. Mirror Symmetry Correlations

Plotting the Hückel π-energy of the chiral fullerenes against the mirror symmetry value [$S(\sigma)$] reveals a remarkable approximate linear correlation between the two (Figures 3, 5, 7, 10). This correlation was found only in enantiomerization reactions of chiral fullerenes and not in automerizations or isomerizations. It may be formulated in the following manner:

$$E^{\pi}_{\text{structure}} = E^{\pi}_{\text{transition state}} - kS(\sigma)_{\text{structure}}; \quad k = \text{const} \quad (10)$$

k behaves much like a force constant of a harmonic oscillator [$F = F(0) - kx$], and therefore, it may be termed an energy-symmetry constant. The linear correlation coefficient may be used as a measure of harmonicity of the potential energy in these reactions. Its value depends on the size of the fullerene and on its structure. The authenticity of this correlation is nicely corroborated by considering the C_{20} fullerene: it is the smallest possible fullerene and it is achiral. Indeed, by extrapolation, one gets $k = 0$ for the C_{20} fullerene (Figure 17). We note also that the linear correlation coefficient may be used as a measure of harmonicity of the potential energy in these reactions.

It is interesting to find that this correlation is identified by the use of the CSM analysis and not by more standard approaches. Thus, one might consider replacing the energy-symmetry constant by

$$k \cong (n - 20)k'; \quad n \text{ is the number of carbons in the fullerene} \quad (11)$$

Unlike Figure 17, plot of the enantiomerization barrier against the fullerene size (Figure 18) shows no predictive pattern.

A possible explanation for the energy-symmetry correlation is that the CSM is a quadratic function of the coordinates. Within simple models, the energy along the reaction path is also a quadratic function (i.e., an inverted harmonic oscillator). Both these functions have extrema at the transition state, hence their correlation. In isomerization and automerization reactions, the system is much more complex. One reflection plane disappears and another appears simultaneously. The distance of the structure to each of the planes goes through a maximum during the course of the reaction. Therefore, a simple correlation between energy and symmetry is less likely for this case, and indeed, it is not found. This hypothesis may be strengthened by examination of the chirality value of the starting cage as a function of the molecule's size (Figure 19). Fullerenes are roughly spherical if we look only at the atom positions. Thus, chiral fullerenes draw their chirality from a common source, namely, their topology. For this reason, given the growth of the normalization factor with the fullerene size, the chirality value decreases as a function of the molecular size. This means that each atom carries less chirality in a larger fullerene so that a greater geometric change is required in order to make an equivalent change in chirality. Such a sizable geometric alteration is translated by the molecule into a large change in energy and hence the monotonic dependence of dE/dS upon cage size. The small differences in energy symmetry constants of fullerenes with an equal number of carbons are attributed to the fine details of the local structural environment of the reacting SW patch.

In summary, we have shown the usefulness of CCM as a reaction coordinate in SW reactions of fullerenes and revealed a predictive pattern for enantiomerization paths. It is possible that such patterns will be found also in other reaction pathways, providing a qualitative tool for predicting their feasibility without explicit and detailed calculation of the energy or geometry of the transition state, once a correlation has been established.

Acknowledgment. We acknowledge support by the German BMBF, the Minerva Foundation, Munich, by the Clore Foundation, and by the British Council.

References and Notes

(1) Stone, A. J.; Wales, D. J. *Chem. Phys. Lett.* **1986**, *128*, 501.
(2) Diederich, F.; Whetten, R. L.; Thilgen, C.; Ettl, R.; Chao, I.; Alvarez, M. *Science* **1991**, *254*, 1768.
(3) Fowler, P. W.; Manolopoulos, D. E.; Ryan, R. P. *J. Chem. Soc. Chem. Commun.* **1992**, *88*, 408.
(4) Fowler, P. W.; Baker, J. *J. Chem. Soc., Perkin Trans. 2* **1992**, 1665.
(5) Manolopoulos, D. E.; Fowler, P. W.; Ryan, R. P. *J. Chem. Soc., Faraday Trans.* **1992**, *88*, 1225.
(6) Hawkins, J. M.; Nambu, M.; Meyer, A. *J. Am. Chem. Soc.* **1994**, *116*, 7642.
(7) Fowler, P. W.; Manolopoulos, D. E. *An Atlas of Fullerenes*; Oxford University Press: Oxford, 1995.
(8) Eckhoff, W. C.; Scuseria, G. E. *Chem. Phys. Lett.* **1993**, *216*, 399.
(9) Murry, R. L.; Strout, D. L.; Odom, G. K.; Scuseria, G. E. *Nature* **1993**, *366*, 665.
(10) Murry, R. L.; Strout, D. L.; Scuseria, G. E. *Int. J. Mass Spectrom. Ion Processes* **1994**, *138*, 113.
(11) Yi, J.-Y.; Bernholc, J. *J. Chem. Phys.* **1992**, *96*, 8634.
(12) Heath, J. R.; O'Brien, S. C.; Curl, R. F.; Kroto, H. W.; Smalley, R. E. *Comments Condens. Matter Phys.* **1987**, *13*, 119.
(13) Manolopoulos, D. E.; Fowler, P. W. In *The Chemical Physics of the Fullerenes 10 (and 5) Years Later*; Andreoni, W., Ed.; Kluwer Academic Press: Dordrecht, 1996.
(14) Heath, J. R. In *Fullerenes: Synthesis. Properties and Chemistry*; Hammond, G. S., Kuck, V. J., Eds.; American Chemical Society: Washington, DC, 1991; pp 1−23.
(15) Fowler, P. W.; Zerbetto, F. *Chem. Phys. Lett.* **1995**, *243*, 36.
(16) Eggen, B. R.; Heggie, M. I.; Jungnickel, G.; Latham, C. D.; Jones, R.; Briddon, P. R. *Science* **1996**, *272*, 87.
(17) Zabrodsky, H.; Peleg, S.; Avnir, D. *J. Am. Chem. Soc.* **1992**, *114*, 7843.
(18) Zabrodsky, H.; Peleg, S.; Avnir, D. *J. Am. Chem. Soc.* **1993**, *115*, 8278 (Erratum: 11656).
(19) Zabrodsky, H.; Avnir, D. *Adv. Mol. Struct. Res.* **1995**, *1*, 1.
(20) Zabrodsky, H.; Avnir, D. *J. Am. Chem. Soc.* **1995**, *117*, 462.
(21) Manolopoulos, D. E.; Fowler, P. W. *J. Chem. Phys.* **1992**, *96*, 7603.
(22) Rassat, A. *C. R. Acad. Sci., Ser. II* **1984**, *299*, 53.
(23) Gilat, G.; Schulman, L. S. *Chem. Phys. Lett.* **1985**, *121*, 13.
(24) Mezey, P. G. *Shape in Chemistry: An Introduction to Molecular Shape and Topology*; VCH Publishers: New York, 1993.
(25) Weinberg, W.; Mislow, K. *J. Math. Chem.* **1995**, *17*, 35.
(26) Seri-Levy, A.; Richards, W. G. *Tetrahedron: Asymmetry* **1993**, *4*, 1917.
(27) Kuz'min, V. E.; Stel'makh, I. B.; Yudanova, I. V.; Pozigun, D. V.; Bekker, M. B. *J. Phys. Org. Chem.* **1992**, *5*, 299.
(28) Luzanov, A. V.; Babich, E. N. *Struct. Chem.* **1992**, *3*, 175.
(29) Hel-Or, Y.; Peleg, S.; Avnir, D. *Langmuir* **1990**, *6*, 1691 (Erratum: **1994**, *10*, 1633).

(30) Meyer, A. Y.; Richards, W. G. *J. Comput. Aided Mol. Des.* **1991**, *5*, 427.

(31) Murray-Rust, P.; Bürgi, H. B.; Dunitz, J. D. *Acta Crystallogr.* **1978**, *B34*, 1787.

(32) Osipov, M. A.; Pickup, B. T.; Dunmur, D. A. *Mol. Phys.* **1995**, *84*, 1193.

(33) Klein, D. J. *J. Math. Chem.* **1995**, *18*, 321.

(34) Buch, V.; Gershgoren, E.; Hel-Or, H. Z.; Avnir, D. *Chem. Phys. Lett.* **1995**, *247*, 149.

(35) Pinto, Y.; Hel-Or, H. Z.; Avnir, D. *J. Chem. Soc., Faraday Trans.* **1996**, *92*, 2523.

(36) Kanis, D. R.; Wong, J. S.; Marks, T. J.; Ratner, M. A.; Zabrodsky, H.; Keinan, S.; Avnir, D. *J. Phys. Chem.* **1995**, *99*, 11061.

(37) Katzenelson, O.; Hel-Or, H. Z.; Avnir, D. *Chem. Eur. J.* **1996**, *2*, 147.

(38) Keinan, S.; Hel-Or, H. Z.; Avnir, D. *Enantiomer* **1996**, *1*, 351.

(39) Avnir, D.; Katzenelson, O.; Keinan, S.; Pinsky, M.; Pinto, Y.; Salomon, Y.; Hel-Or, H. Z. In *Concepts in Chemistry: A Contemporary Challenge*; Rouvray, D. H., Ed.; Research Studies Press Ltd.: Taunton, Somerset, England, 1997; pp 283−324.

(40) Avnir, D.; Hel-Or, H. Z.; Mezey, P. G. In *Encyclopedia of Computational Chemistry*; Schleyer, P. v. R., Ed.; Wiley: Chichester; in press.